Addressing the Hypersonic Simulation Problem

B. J. Griffith,* J. R. Maus,† and B. M. Majors‡
Calspan Corporation, Arnold Air Force Station, Tennessee
and
J. T. Best§
Arnold Engineering Development Center, Arnold Air Force Station, Tennessee

The hypersonic simulation problem is solved by the meshing of bench-marked experimental data with results from validated computational fluid dynamic codes. The example presented is for the re-entry of the Space Shuttle Orbiter. Mach number effects were assessed by parametrically varying the freestream Mach number and angle of attack in a series of inviscid, perfect-gas computations carried out on a modified Orbiter geometry. Real-gas effects were determined by making calculations at specific points of the re-entry trajectory using equilibrium air thermodynamics and comparing them with corresponding perfect-gas computations. Viscous computations were also made for both the basic Orbiter body and the control surfaces. A methodology is developed that permits the extrapolation of wind tunnel data to flight situations, providing a solution to the hypersonic simulation problem.

Nomenclature

A	= reference area, 2,690 ft^2
CG	= orbiter center of gravity
C_M	= pitching-moment coefficient, M_0/cAq_∞
C_N	= normal-force coefficient, F_N/Aq_∞
C_∞	= viscosity parameter
c	= reference length, 474.8 in.
EV	= elevon deflection, deg
F_N	= normal-force component
K	= constant
L	= body length, 1,293 in.
M_0	= total moment about $x_0 = 840.7$ in., $z_0 = 37.0$ in.
M_∞	= Mach number
q_∞	= dynamic pressure
$Re_{\infty L}$	= freestream Reynolds number based on model length
$\bar{V}_\infty$	= viscous parameter, $M_\infty \sqrt{C_\infty}/\sqrt{Re_{\infty L}}$
x,y,z	= Cartesian coordinates
x_0,z_0	= location of orbiter CG
α	= angle of attack
ΔC_{A_v}	= basic body viscous axial force
ΔC_M	= incremental pitching moment
ΔC_{M_v}	= basic body viscous pitching moment
ΔC_N	= incremental normal force
$\Delta C_{N_I}, \Delta C_{M_I}$	= incremental normal force and pitching moment for the basic body attributable to real gas and Mach number
ΔX_{cp}	= incremental center of pressure
δ_{BF}, BF	= body-flap deflection, deg
γ	= specific heat ratio

Presented Paper 86-9775 at the AIAA/AHS/CASI/DGLR/IES/ISA/ITEA/SETP/SFTE 3rd Flight Testing Conference, Las Vegas, NV, April 2-4, 1986; received April 21, 1986; revision received Sept. 29, 1986.

*Calspan Consultant, presently Senior Staff Engineer, RADG, Huntsville, AL. Associate Fellow AIAA.
†Senior Staff Engineer, AEDC Division. Member AIAA.
‡Computer Scientist, AEDC Division.
§Program Manager, U.S. Air Force. Member AIAA.

Introduction

THE Wright brothers built a low-speed wind tunnel to simulate the flow over their airplane and made history in 1903 by making a manned flight last 59 s. Chuck Yeager broke the sound barrier in 1947 with the help of transonic wind tunnel tests that did not fully simulate the flight of his Bell X-1 because of tunnel wall effects and a lower than desired Reynolds number. Scott Crossfield flew a D-558-2 on Nov. 20, 1953 and became the first person to travel at twice the speed of sound without fully knowing the aerodynamic loads because of a lack of proper ground test simulation.

Time has not improved the ground test simulation of flight. In fact, ground test facilities are less able to simulate today's high-speed flight than the flight speeds encountered by the Wright brothers, Yeager, or Crossfield. A recent example is the re-entry of the Space Shuttle Orbiter.

The re-entry of the Space Shuttle Orbiter has been remarkably successful; only a few problems or anomalies have arisen during the various flights to date. One problem has resulted from a significant difference between preflight predictions of hypersonic pitching moment and values inferred from flight data.[1-3] These differences have resulted in body flap deflections required to maintain trim more than twice those predicted prior to STS-1.

This paper presents an analysis of the flight data, ground test, and computational results used to resolve this discrepancy. Some of the fundamental flow modeling necessary to extrapolate ground test data to hypersonic flight conditions is presented. In particular, this paper documents the high Mach number, real-gas, and viscous effects on the Orbiter aerodynamics, plus flight and tunnel data problems.

Mach number effects were assessed by parametrically varying the freestream Mach number and angle of attack in a series of inviscid, perfect-gas computations carried out on a modified Orbiter geometry. Real-gas effects were explored by making calculations at specific points of the re-entry trajectory using equilibrium air thermodynamics and comparing the predictions with corresponding perfect-gas computations. Viscous effects on the Orbiter aerodynamics were determined by an analysis of wind tunnel heat transfer and viscous drag data supplemented by several viscous computations at low angles of attack. Body flap and elevon effectiveness have also been examined by the use of ground test and flight test data with a limited amount of computational results.

Approach

Figure 1 illustrates the approach taken in the simulation process. The synergistic combination of experimental aerodynamics, basic aerodynamic simulation concepts, and computational fluid dynamics is required. Feedback from flight data permits the fine-tuning of the simulation procedure.

Computational modeling requires that all variables be considered, since some variables are additive and others subtract from the experimental data base. The list of variables considered during the present study is given in Fig. 1. Figure 2 illustrates the simulation problem. Note the Mach number and viscous regime of the flight of STS3 not covered by AEDC Tunnel B. Other facilities would provide slightly higher Mach numbers but would still be perfect-gas facilities and suffer somewhat in data precision. A 1% error in center-of-pressure results in over a 12-in. uncertainty in the full-scale Orbiter center of pressure. Therefore, data from AEDC Tunnel B at Mach 8 were selected as the bench mark to be coupled with computational fluid dynamic (CFD) solutions. The approach as shown in Fig. 3 also involves fine-tuning the prediction methodology with flight results. The high quality of the STS flight data not only allowed the fine-tuning of the prediction methodology, but flight trends suggested several shortcomings of 1) the initial analysis, 2) the flight data, and 3) the tunnel data: each will be discussed herein.

Detailed Simulation Procedure

The detailed simulation procedure is shown in Fig. 4. The steps in the procedure are briefly listed as follows:

1) Analyze flight and tunnel data for possible corrections.

2) Compute changes in basic body aerodynamics attributable to Mach number, real-gas, and viscous effects.

3) Compute changes in control surface deflection caused by Mach number, real-gas, viscous, and flexibility effects.

4) Develop methodology for comparing tunnel data and CFD results with flight data.

5) Fine-tune methodology as suggested by the flight data.

Flight Data Analysis

The Shuttle flight test program has produced the highest quality and most extensive aerodynamic data base ever collected. The major shortcoming of the data base is a lack of precise knowledge of the atmospheric density, particularly at high altitudes. A second problem is knowing the center of gravity to better than ±3/4 in., which adds to the analysis problem. However, the extensive data base permits these two problems to be considered as data scatter and not as a flight bias.

A detailed inspection of the flight data from several flights indicates a trend with the body flap that suggested a body-flap flexibility problem not accounted for in the Aerodynamic Design Data Book (ADDB).[1] Figure 5a gives some preflight loading data that were not used in the ADDB. Including these data in the flight analysis gives for a windward body flap a lower deflection and for a leeward body flap a higher deflection than recorded. Typical corrections are presented in Fig. 5b. These corrections are included in the methodology model.

Tunnel Data Analysis

The ground test program of the Space Shuttle was extensive (see Fig. 6). Nearly all of the hypersonic ground test facilities

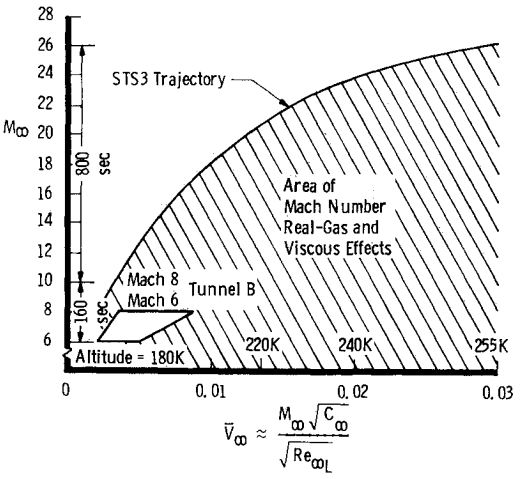

Fig. 2 Illustration of simulation problem.

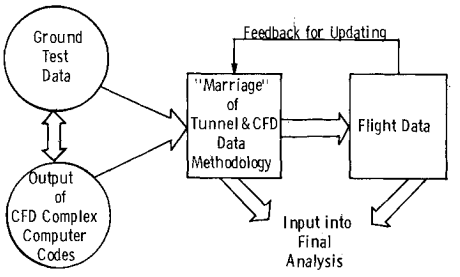

Fig. 3 Approach of simulation.

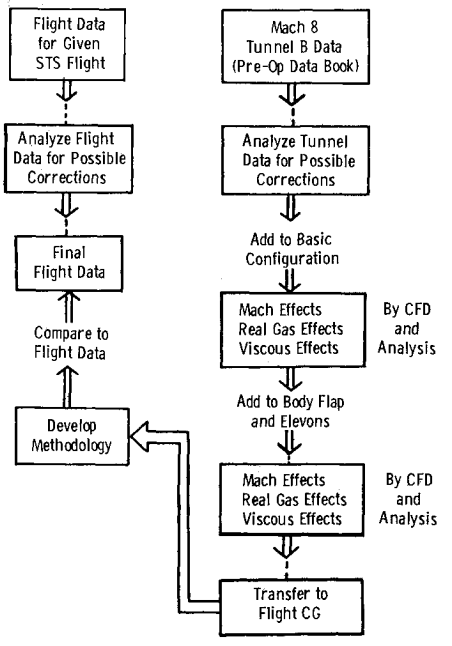

Fig. 4 Detailed simulation procedure.

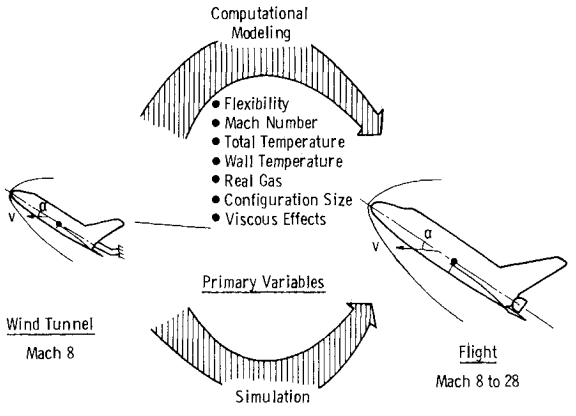

Fig. 1 Overview of simulation methodology.

were utilized, and data were reviewed by experts from Langley, Ames Research Center, Johnson Space Center, and Rockwell to establish the most valid set of wind tunnel data.[2] Ground test data above Mach 10 were not of sufficient quality to define the moment characteristics of the Orbiter. A high-fidelity 0.02-scale model was built and tested in AEDC Tunnel B in order to update the Aerodynamic Design Data Book. Tunnel B is a validated facility that produces high-quality data. These data resulted in the Pre-op Aerodynamic Design Data Book,[3] which only slightly changed the original data set. The wind tunnel results were not adjusted for real-gas effects.

The Tunnel B test series were designated 0A258. The sting deflection constants were carefully derived in both the balance lab and in the tunnel (air off). Extensive checks were made in order to obtain high-quality data. The model was also run upright and inverted in order to isolate any tunnel flowfield effects. A close inspection of the data at various dynamic pressures and test entries revealed some trends not noted during the earlier data analysis. The normal force at a constant angle of attack slightly increased as the dynamic pressure increased, indicating a model/sting/sector bending problem not accounted for in the original data reduction. Figure 7 shows the revised data compared to the ADDB[3] data ($M_\infty = 8$). The normal force (C_N) is decreased about 4%, giving a small nose-up moment.

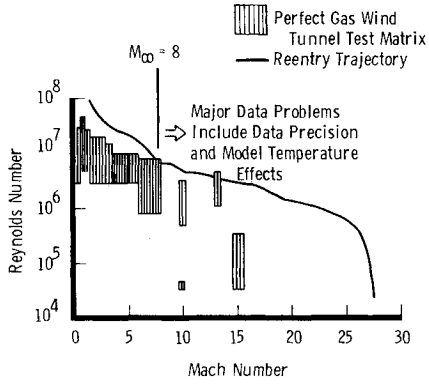

Fig. 5 Analysis of STS flight body-flap flexibility effects: a) Rockwell's body-flap flexibility data and b) body-flap flexibility corrections.

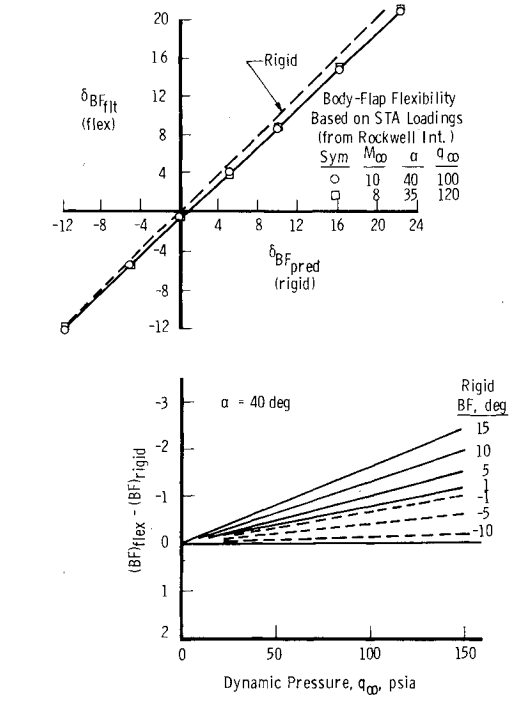

Fig. 6 Orbiter wind tunnel data base.

Basic Body Aerodynamics

The computational results have been presented in previous works (for details, see Refs. 4–7). A synopsis will be given in this paper.

The applicable flow regimes of the various computational codes are shown in Fig. 8. Six advanced CFD codes[8–13] have been applied to a modified Orbiter geometry to obtain detailed viscous and inviscid flowfield solutions. Solutions were obtained for wind tunnel conditions to validate the computational results and for hypersonic flight conditions. Figure 9 presents a sketch of the Orbiter and Fig. 10 illustrates the geometry for which the computations were performed. The major differences between the inviscid computational model and the actual Orbiter geometry are as follows: 1) the wing sweepback angle has been increased from 45 to 55 deg, 2) the wing thickness of the model is about twice that of the Orbiter, 3) the computational geometry is squared off at the body-flap hinge line, and 4) the rudder and OMS pod are not included in the model geometry. The computational geometry was obtained from NASA/LaRC and was not altered during the course of this investigation. An elliptical upper surface was added to create the viscous model. These modifications were necessary in order to obtain CFD solutions for this complex body.

Code Validation

To establish the credibility of the CFD results and to assess the effect of geometrical differences on the aerodynamic parameters, initial computations with CM3DT and STEIN were made to compare with wind tunnel results. The specific wind tunnel data used in this comparison are from AEDC Tunnel B. A comparison of the computed and experimental normal-force coefficients is shown in Fig. 11.

Predicting the pitching moment is a severe test for any CFD code. Figure 12 shows a comparison of the computed pitching-

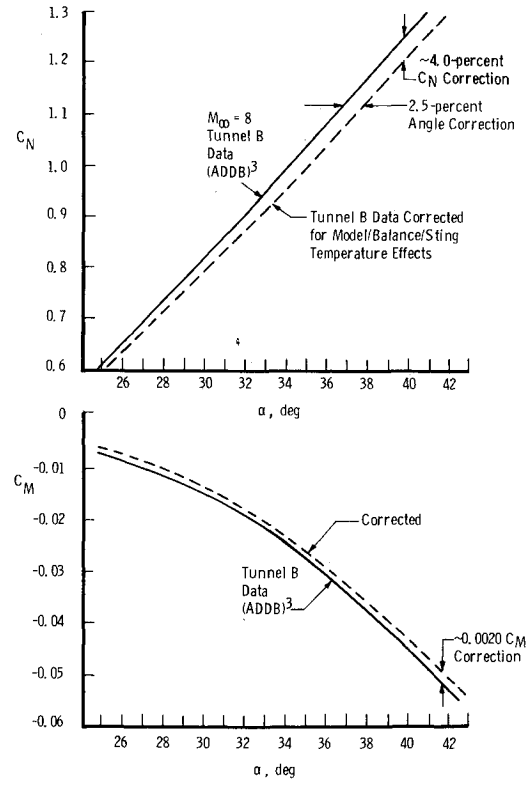

Fig. 7 Analysis of AEDC tunnel experimental data.

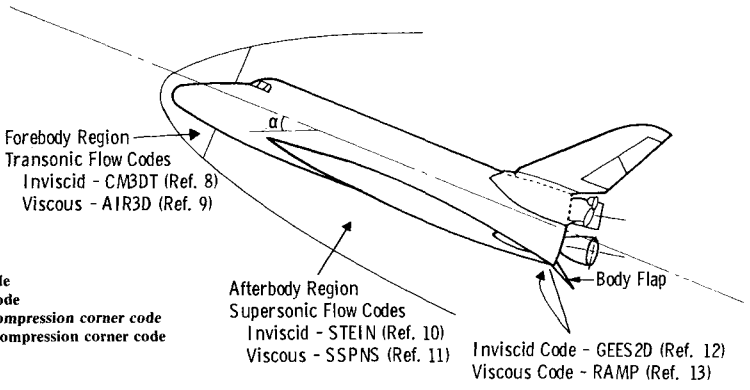

Fig. 8 Computational regimes of various codes.

AIR3D: three-dimensional viscous blunt-body code
CM3DT: three-dimensional inviscid blunt-body code
GEES: two-dimensional inviscid time-marching compression corner code
RAMP: two-dimensional viscous time-marching compression corner code
SSPNS: viscous space-marching afterbody code
STEIN: inviscid space-marching afterbody code

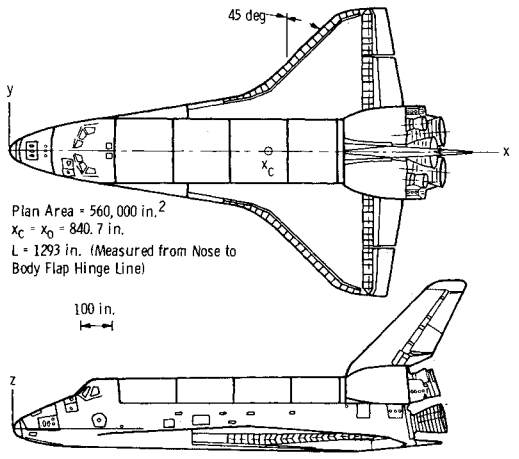

Fig. 9 Shuttle Orbiter geometry.

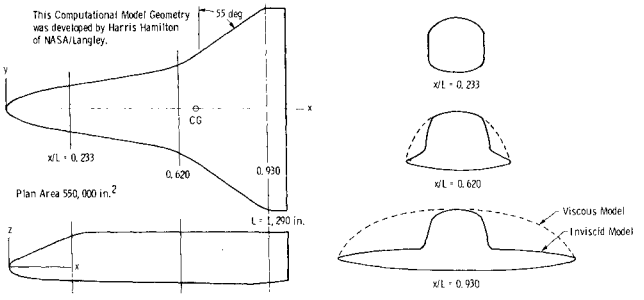

Fig. 10 Computational model geometry.

moment coefficient with the experimental values for the basic Orbiter geometry. The maximum deviation, which occurs at an angle of attack of about 30 deg, corresponds to a difference in the center of pressure of only 0.3% of the body length, indicating that the computational model is a realistic representation of the actual Space Shuttle Orbiter.

The results of these comparisons give confidence in the applicability of the computational code to the complex model Orbiter geometry. These CFD codes and a set of high-quality Mach 8 tunnel data are the tools used to develop a hypersonic simulation model.

Real-Gas and Mach Number Effects

Real-gas effects on the normal-force coefficient of the Space Shuttle Orbiter model are illustrated in Fig. 13. The Mach numbers for the real-gas computations in this figure correspond to points of the Orbiter re-entry trajectory. Figure

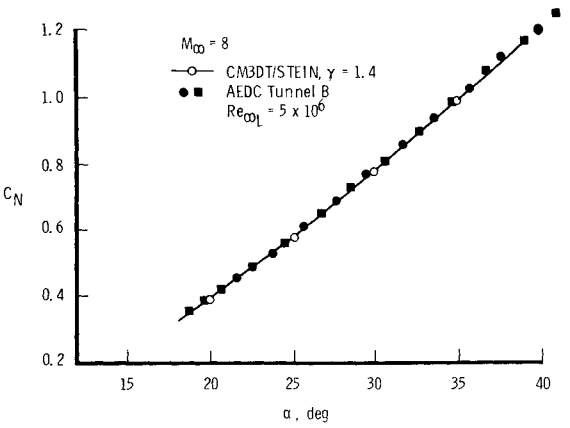

Fig. 11 Comparison of computed normal-force coefficient with experimental data.

13 indicates a slight decrease in the normal-force coefficient, attributable to real-gas effects caused by the lower pressures on the aft part of the Orbiter.

Real-gas effects on the pitching moment are illustrated for a high-velocity, high-altitude trajectory point in Fig. 14 by comparing the results for perfect-gas computations with those for equilibrium-air thermodynamics. This figure reveals that the real-gas effects drive C_M more positive, with the effects being most significant at high angles of attack.

The combined Mach number and real-gas effects are illustrated in Fig. 15 for the high- Mach number conditions, in terms of the forward shift of the aerodynamic center of pressure from the baseline, $M_\infty = 8$, perfect-gas case. This figure shows that the shift in the center of pressure is about 12 in. forward for an angle of attack of 35 deg and about 21 in. forward for an angle of attack of 20 deg, resulting in significant changes in the aerodynamics of the Shuttle.

The combined correction of C_N and C_M attributable to inviscid Mach number and real-gas effects is shown in Fig. 16 as a function of the angle of attack (α) and Mach number. Three significant factors should be noted. These are: 1) there is a loss in normal force (C_N) attributable to high- Mach number and real-gas effects, 2) at the angle of attack of 40 deg, the Mach number and real-gas effects on C_M at re-entry Mach numbers are about 0.0300 (nose up), and 3) at Mach 8 (baseline condition) there is a small, yet significant, real-gas effect that is not included in the data base.

Viscous Effects

Simple approximate analytical expressions for the viscous contributions to C_A and C_M have been derived to supplement PNS solutions and permit extrapolation of those results to higher angles of attack. The derivation and validation of these expressions and the results of the PNS solutions are given in

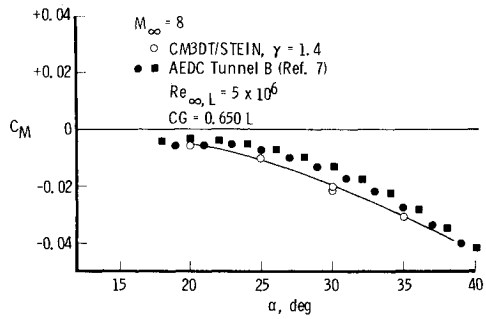

Fig. 12 Comparison of computed pitching-moment coefficient with experimental data.

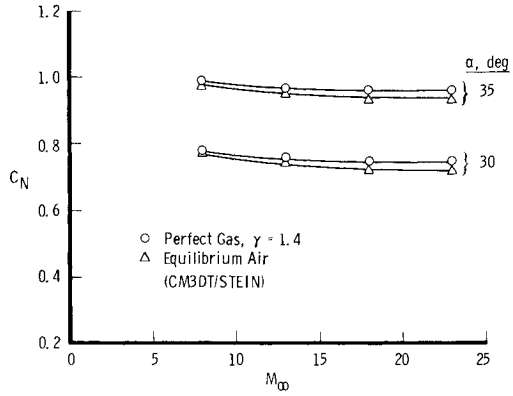

Fig. 13 Real-gas effect on normal-force coefficient.

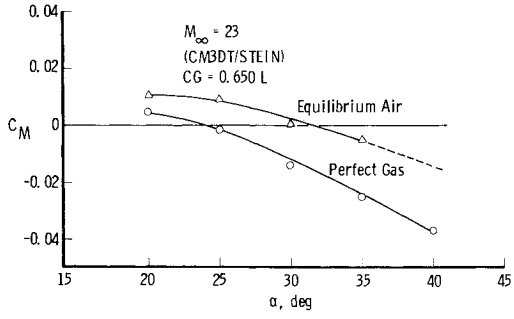

Fig. 14 Real-gas effect on pitching-moment coefficient.

Ref. 5. The analytical expressions are

$$\Delta C_{A_v} = 3.63 \bar{V}_\infty \sin\alpha\,(\cos\alpha)^{1.75} \quad (1)$$

$$\Delta C_{M_v} = -0.765 \bar{V}_\infty \sin\alpha\,(\cos\alpha)^{1.75} \quad (2)$$

An examination of Eq. (2) indicates that viscous effects on the basic Orbiter body cause a nose-down movement.

Control Effectiveness

An investigation of the control-surface effectiveness was carried out in a manner similar to that performed on the basic vehicle itself. The body flap and elevons were modeled as two-dimensional compression corners, and computations of the flowfield were made using time-marching inviscid and viscous CFD codes. Figure 17 presents a sketch of the computational method and the CFD codes used in the analysis. No significant Mach number effect was found for either the body flap or elevons (less than 5% of the moment contribution attributable to the body flap).

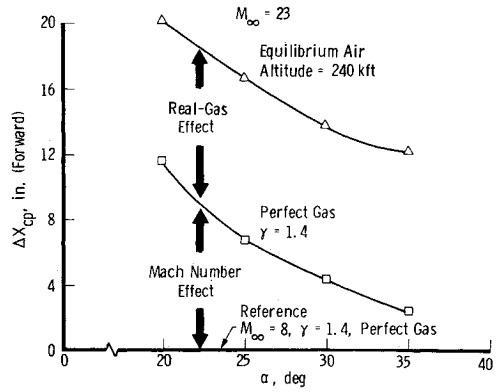

Fig. 15 Combined Mach number and real-gas effects on center-of-pressure location.

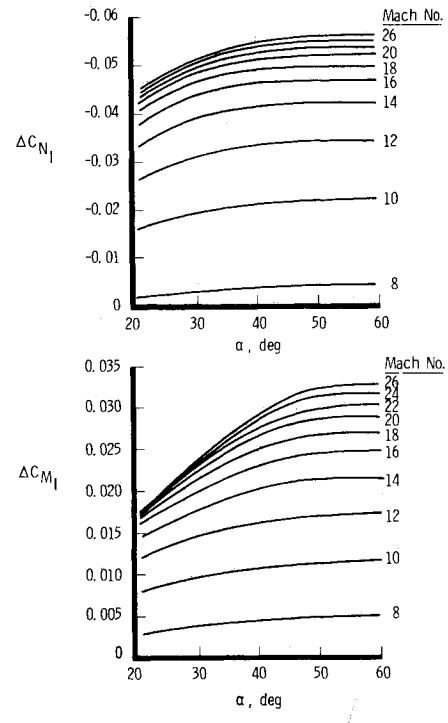

Fig. 16 Combined Mach number and real-gas effects on C_N and C_M.

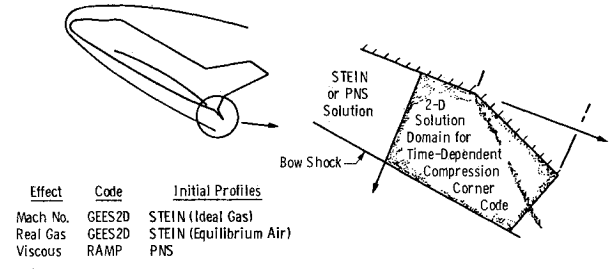

Fig. 17 Control surface investigation, computational domain and codes.

Real-Gas Effects

Limited computations for the influence of real gas on the body flap at Mach 23 are presented in Ref. 7. The computations were made for an altitude of 240 kft. The computational data were modeled by assuming a variation with Mach numbers (hence altitude) and angle of attack identical to the basic body real-gas effect on C_M (see Fig. 16). The results are shown in Fig. 18 for the STS3 trajectory. Since all the trajec-

tories are somewhat similar, this curve can be utilized for any present STS trajectory. Note that real-gas effects increase the body-flap effectiveness.

A similar study was made on the elevons. The results indicated that the maximum effect of real gas was less than 5% of the moment contribution attributable to the elevons.

Viscous Effects

The influence of viscosity on the body flap was also computed and modeled. A substantial loss of effectiveness is shown in Fig. 18 at Mach 23 and an altitude of 240 kft. The CFD data were modeled using the method derived in Ref. 14, which included the effect of entropy-layer swallowing. Therefore,

$$(\Delta C_{M_v})_{BF} = f[K/(Re_{\infty L})^{1/3}] \quad (3)$$

Figure 18 presents the loss in body-flap effectiveness along the STS3 trajectory. This curve is also good for all trajectories to within ±2%. Computations made for the elevons indicate the loss in effectiveness is only 50% of the loss incurred by the body flap.

Simulation Methodology Compared with Flight Data

Some results of the simulation procedure as outlined in Fig. 4 are presented in Figs. 19 and 20. Figure 19 shows a comparison of the rigid body-flap deflection from flight STS1 and the methodology model. The methodology model considers the body-flap flexibility corrections shown in Fig. 5. The comparison shown in Fig. 19 is the maximum deviation of any of the nine flights considered. Also shown in this figure is the preflight prediction of the required body-flap deflection computed using Ref. 1.

A summary of the flight normal force (C_N) compared to the CFD computations is shown in Fig. 20. The CFD computations give an excellent representation of the flight data.

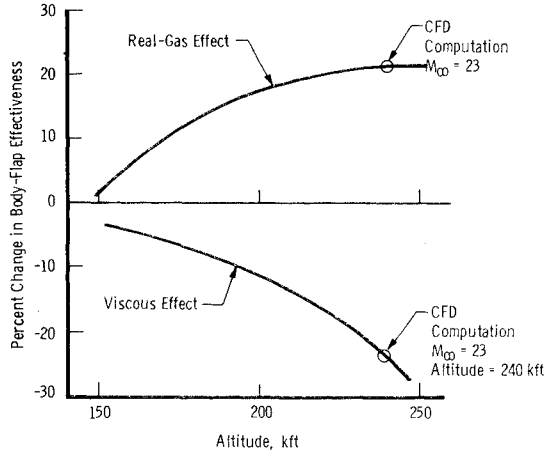

Fig. 18 Computed real-gas and viscous effects on body flap, STS3 flight.

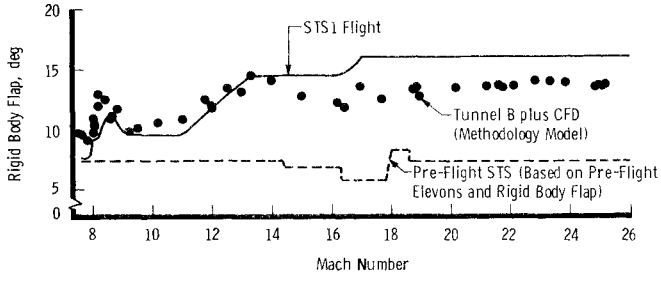

Fig. 19 Comparison of simulation methodology with STS1 flight data.

Simulation Model Updated with Flight Data

The comparison of the simulation methodology with the flight data presented in Fig. 19 shows substantially better agreement than the preflight predictions. Despite the improved agreement, deficiencies in the methodology are still apparent, particularly in the pitching moment and/or control effectiveness. The extensive flight data base for the Shuttle Orbiter permitted a re-examination, assessment, and modification of the various components that comprise the simulation model as illustrated in Fig. 3. Several regression studies were made using data from the first nine flights and the simulation model in the following order:

1) Data below 220 kft where the body flap was near zero—Within this data bank, the only component of the simulation model that should vary would be the basic body real-gas and Mach number model. The basic body viscous effects within this data bank would be insignificant.

2) Data near Mach 8—To update the body-flap flexibility effects. All other components of the simulation model should not vary.

3) Data between Mach 8 and Mach 18—To update the real-gas and Mach number effects on the body flap. The remaining components of the simulation model were not allowed to change.

4) Data between Mach 18 and 25 (≈ 250 kft)—To update the viscous effects on the body flap.

Each regression analysis used the updated simulation model from the previous analysis.

Modification of the Basic Body and Real-Gas Effects

The regression analysis from the data where the body flap was near zero was used to update the basic body real-gas and Mach number model. These results are shown in Fig. 21. There are several possible reasons why a flight adjustment is necessary. The most likely would be the differences between the actual flight vehicle and the computational model.

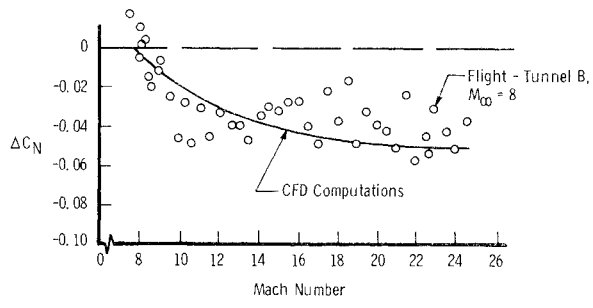

Fig. 20 Summary of STS3 flight analysis, C_N.

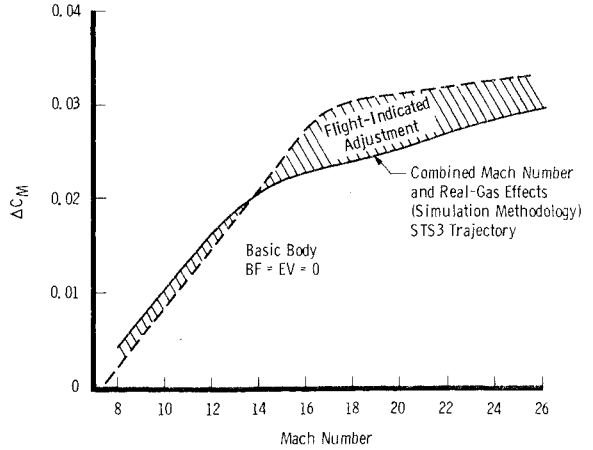

Fig. 21 Flight-indicated adjustment to basic body Mach number and real-gas effects.

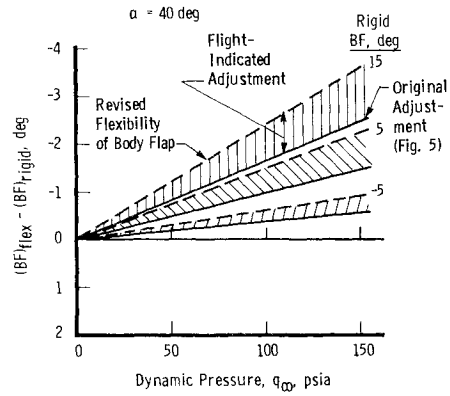

Fig. 22 Flight-indicated adjustment to body-flap flexibility effects.

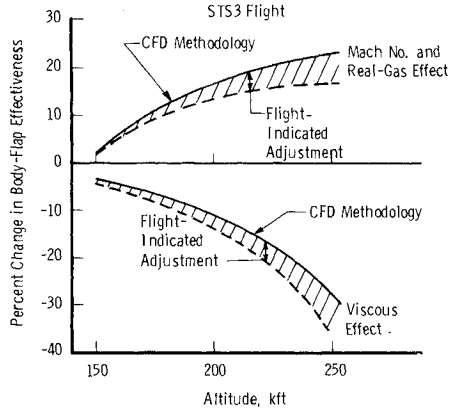

Fig. 23 Flight-indicated adjustment to body-flap, real-gas, and viscous effects.

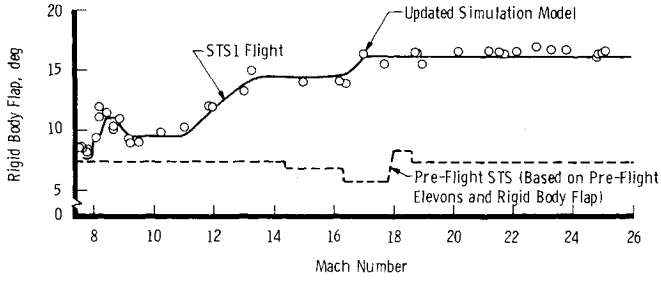

Fig. 24 Comparison of updated simulation methodology with STS1 flight data.

Modification of the Body-Flap Flexibility Effects

The regression analysis near Mach 8 was used to update the body-flap flexibility effects. The logic was that 1) the influence of real gas would be small, 2) viscous effects would be very small, and 3) the consistency of the ground test data indicated that no problem existed with this data base. Figure 22 shows the updated body-flap flexibility corrections.

Modification of the Body-Flap Real-Gas and Mach Effects

The flight data between Mach 8 and 18 were used to update the real-gas and Mach effects on the body flap, since viscous effects in this regime are small. The analysis (Fig. 23) indicated that the computational results overpredict the body-flap effectiveness.

Modification of Body-Flap Viscous Effects

Viscous effects become important for the STS trajectories at about Mach 18 and above. A regression analysis on the flight

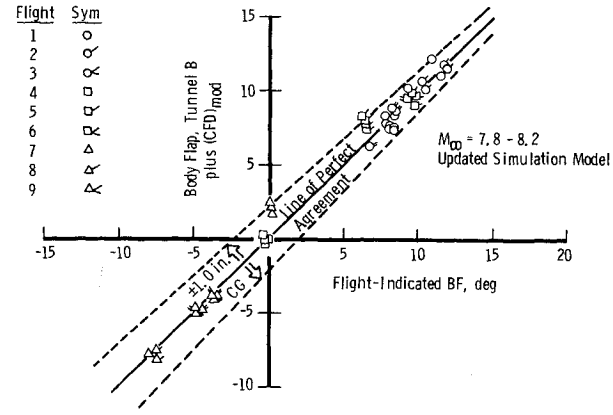

Fig. 25 Comparison of indicated and computed body flap, $M_\infty = 7.8$–8.2.

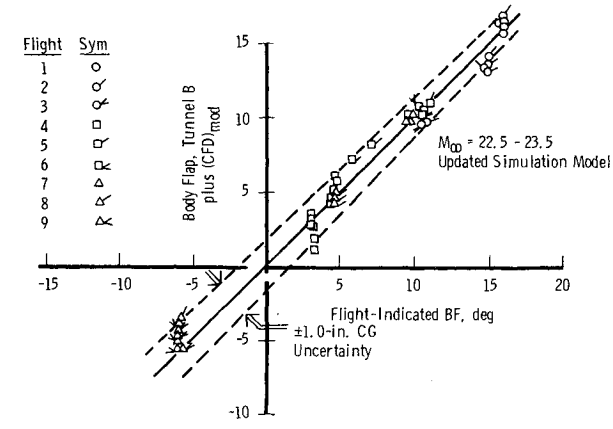

Fig. 26 Comparison of indicated and computed body flap, $M_\infty = 22.5$–23.5.

data in this region indicates that the computational results underpredict the loss of body-flap effectiveness as shown in Fig. 23.

Updated Simulation Model Compared with Flight Data

Comparisons of the updated simulation model and the STS flight data are shown in Figs. 24–26. Figure 24 shows the improved agreement with STS1 data at various points along the trajectory. Figures 25 and 26 give a comparison near Mach 8 and Mach 23 with the first nine STS flights. Also shown is the variation that ±1.0 in. in the Orbiter center of gravity would give. The updated simulation model is in excellent agreement with the flight data.

Concluding Remarks

A methodology model has been developed using benchmark wind tunnel data and advanced CFD codes for the Space Shuttle Orbiter above 150 kft. The methodology model has been updated using flight results and gives excellent results.

The same approach could be used for any other flight vehicle. The main restriction with this approach is that each methodology model is configuration-limited. However, the advances in ground testing, computational fluid dynamics, and scientific computations make this approach very attractive, especially for less complex bodies. CFD solutions for simple geometries are less demanding, and the matrix of computational conditions can be relatively sparse. The authors have used this approach for several Air Force re-entry vehicles with excellent results.

The three main requirements are 1) a reliable set of wind tunnel data, 2) validated CFD codes, and 3) a careful assessment of all the known variables that could affect the vehicle re-entry.

Acknowledgments

This study was sponsored by the NASA Johnson Space Center and Arnold Engineering Development Center. The authors wish to express appreciation to Mr. J. M. Underwood and P. O. Romere of NASA/JSC for their assistance and advice throughout the study.

References

[1]"Aerodynamic Design Data Book, Volume 1M, Orbiter Vehicle," edited by W. R. Russell, Rockwell International, SD72-Sh-0060, Oct. 1978.

[2]Young, J. C., et al. "Space Shuttle Entry Aerodynamic Comparisons of Flight 1 with Preflight Predictions," AIAA 81-2476, Nov. 1981.

[3]"Pre-Operational Aerodynamic Design Data Book, Volume IL, Orbiter Vehicle," edited by W. R. Russell, Rockwell International, SD72-SH-0060, April 1982.

[4]Maus, J. R., Griffith, B. J., Szema, K. Y., and Best, J. T., "Hypersonic Mach Number and Real-Gas Effects on Space Shuttle Orbiter Aerodynamics," *Journal of Spacecraft and Rockets*, Vol. 21, March/April 1984, pp. 136-141.

[5]Szema, K. Y., Griffith, B. J., Maus, J. R., and Best, J. T., "Laminar Viscous Flow-Field Predictions of Shuttle-Like Vehicle Aerodynamics," AIAA Paper 83-0211, Jan. 1983.

[6]Griffith, B. J., Maus, J. R., and Best, J. T., "Explanation of the Hypersonic Longitudinal Stability Problem—Lessons Learned," NASA Langley Conference on Shuttle Performance—Lessons Learned, Hampton, VA, March 1983.

[7]Maus, J. R., Griffith, B. J., Tolbert, D. J., and Best, J. T., "Understanding Space Shuttle Flight Data by Use of Wind Tunnel Data and CFD Results," AIAA Paper 83-2745, Nov. 1983.

[8]Hall, D. W., "Inviscid Aerodynamic Predictions for Ballistic Reentry Vehicles with Ablated Nosetips," Science Applications, Inc., SAI-79-506-VF, Feb. 1979.

[9]Kutler, P., Pedelty, J. A., and Pulliam, T. H., "Supersonic Flow Over Three-Dimensional Ablated Nosetips Using an Unsteady Implicit Numerical Procedure," AIAA Paper 80-0063, Jan. 1980.

[10]Marconi, B., Salas, M., and Yaeger, L., "Development of a Computer Code for Calculating the Steady Super/Hypersonic Inviscid Flow Around Real Configurations," NASA CR-2675, April 1976.

[11]Schiff, L. B. and Steger, J. L., "Numerical Simulation of Steady Supersonic Viscous Flow," AIAA Paper 79-0130, Jan. 1979.

[12]Unpublished, developed by Dr. R. G. Hindman, Iowa State Univ. under contract to Calspan/AEDC Division for the Air Force.

[13]Hindman, R. G., "Modifications to MacCormack's 2-D Navier Stokes Compression Ramp Code for Application to Flows with Axes of Symmetry and Wall Mass Transfer," AEDC-TR-80-24 (AD-A093742), Jan. 1981.

[14]Adams, J. C. Jr., Martindale, W. R., Mayne, A. W. Jr., and Marchand, E. O., "Real Gas Scale Effects on Hypersonic Laminar Boundary Layer Parameters including Effects of Entropy Layer Swallowing," AEDC-TR-75-2 (AD-A0187755), Dec. 1975.